

9 Two-strategy two-person decision processes

Based on our work in the last chapter, we have sufficient grounding to specify the *known behaviors*. The reasonableness of this specification may not be entirely obvious until we have worked out a few examples. In thinking about what examples to pick, we note that game theory practitioners are familiar with a large number of two-person zero sum games. There is a large literature around such games. Many of those games for simplicity have been reduced to ones in which each player has just two strategies. This seems to be a good place to start.

In this chapter, we consider two players, each of which has two strategies and assume that the players agree to a *code of conduct* in which the sum of all strategies is inactive; thus we have three active strategies. We explore *harmonic solutions*, section 4.5.7, based on the *player fixed frame model*. This still leaves many possible solutions. This model framework provides significant insight into both the vorticity *free fall harmonic* behaviors and the *system response harmonics*.

As a specific game, we choose one of the examples from chapter 7, exercise 6, which is the attack-defense game from (Williams, 1966). The details for how to deal with such models has been given in the previous chapter. For example, the preliminary transformation Eq. (8.58) can be done as exercise 28, section 8.12, which also provides the null vector Eq. (8.89).

9.1 Attack-Defense model

We recall that the attack-defense game posits that “Blue has two installations. In normal form, he is capable of successfully defending either of them, but not both; and Red is capable of attacking either but not both. Further one of the installations is three times as valuable as the other.” The attack or defense of the lesser installation is labeled “one,” the other is “two.” The payoff matrix for blue is:

$$G_{Blue} = \frac{1}{10} \begin{pmatrix} 4 & 1 \\ 3 & 4 \end{pmatrix} \quad (9.1)$$

There are a number of assumptions involved at this early stage that need to be highlighted. In arriving at the payoff matrix, the argument is made that one installation is three times more valuable than the other. Hence to “Blue”, a defense of the less valuable installation and a corresponding attack on that installation is worth 3+1 units. If the attack is made on the more valuable installation, “Blue” sees only 1 unit of value. Similarly, an attack on the lesser installation while defending the valuable has a value 3 units while an attack on the more valuable one (and defending it) is worth again 3+1 units. The numbers make sense, but remember that in game theory any other payoff matrix in which we change the scale or add a constant will have the same strategic consequences. In *decision process theory* this is no longer the case, so we consider as dynamic the scale factor and additional constants.

We scale the payoff for “Blue” by $\frac{1}{10}$. This changes the model. We make a different argument for “Red” and consider the following payoff:

$$G_{Red} = \frac{1}{10} \begin{pmatrix} 0 & 1 \\ 2 & 0 \end{pmatrix} \quad (9.2)$$

We argue that if “Red” attacks the lesser of the two targets and it is defended, there is no value; similarly if “Red” attacks the other target and it is defended. “Red” actually gets pleasure or reward of 1 unit if the attack is made on the lesser target and it is undefended. The reward is 2 units if the attack is made on the

greater value target and it is undefended. The payoff matrix here is from “Red’s” point of view. For our numerical work we scale “Red” payoffs by $\frac{1}{10}$.

We don’t have a zero-sum game but a constant sum game. Each player sees a positive expected payoff. What we see in the numerical results is a difference in the dynamics for the game as stated and the zero-sum game implicitly implied by the original problem statement. The rule in *game theory* is that nothing depends on a linear scale transformation; this is not true in *decision process theory*. The first conclusion is that the scale changes the “size” of the strategy space; the smaller the scale the larger the effective space. We have scaled down by a factor and get a space that has approximately unit size.

We lay out the behavior in the following subsections for this model and our choice of parameters, which reflects primarily a free fall behavior (section 8.7). We elaborate on other models in the exercises at the end of the chapter (section 9.5). Of particular interest will be a slight variant of the free fall model where we add a small acceleration behavior with a characteristic frequency about half that of the free fall frequency. We proceed now to the details of the model behavior.

9.2 Locked behaviors

In the prisoner’s dilemma, we found that the elastic force populated a high pressure zone, Figure 5-3. Associated with this behavior was a characteristic rise in the acceleration gradient, Figure 5-4. In the inquiry into behaviors for 2+1 dimensions we again found corresponding behaviors in Figure 8-3 and Figure 8-4, which we characterized as **locked behavior**. It has been found in other fields, such as the study of weather phenomena, that there is value in focusing on areas of high pressure and low pressure. Based on the locations of the highs and lows we then get a more complete picture of the overall behavior patterns. For that reason we believe that looking for the cause of *locked behavior* may be fruitful.

For the, the attack-defense model, the parameter choices by themselves don’t lead to the locked behavior observed in the aforementioned references. In fact the initial choice of parameters lead to a pressure that is negative. We see from Eq. (8.19) that terms contribute with both signs. Our analogy to physical systems suggests that the average pressure and the energy density should both be positive (Hawking & Ellis, 1973). An elastic system is usually thought to be one that resists being pressed. A positive energy density is usually thought to be related to the causality of the system; effects occur after causes. If our initial parameter choices generate a negative pressure, the solution is to modify those parameter choices by increasing the size of one or more terms that provide positive contributions. We call solutions that everywhere have positive pressure and energy density solutions with **locked behaviors**.

There are several ways we can provide positive contributions: we can add elastic pressures π^β_β , which are currently set to zero; as with the prisoner’s dilemma we can add strong compression terms $\Theta \cdot \Theta$; we can add rotational terms $\omega \cdot \omega$, which is a classic way to balance negative pressure or collapse; or we can add *player interest* terms $-\mathbf{I}_a \cdot \mathbf{I}^a$, which also generate rotational effects. All of these provide positive contributions to the pressure and would generate locked behaviors. We have chosen to generate our numerical examples by increasing the *player interest*. We do this by increasing the *strategy bias field* f^j_{ov} for each player. We get a result that operates symmetrically on each player. From the model considerations Eq. (8.58), this corresponds to lowering the parameter m^j for each player. We find that we must lower these values sufficiently so that the null space vectors for each payoff are no longer time-like but space-like. We see no inconsistency in this however. There is still a time like vector that defines the flow of energy momentum. The result is that we have a force in the co-moving frame that traps the behaviors and generates a strong *player interest* for each player. This effect we believe is observable: we will see that we generate a player interest that increases for Red and decreases for Blue as player 1 (Blue) becomes dominant $z > 0$.

Thus for a sufficiently strong player strategy bias field f^j_{ov} , we obtain the following **locked behaviors** for the pressure (Figure 9-2) and the acceleration (Figure 9-1).

The Dynamics of Decision Processes

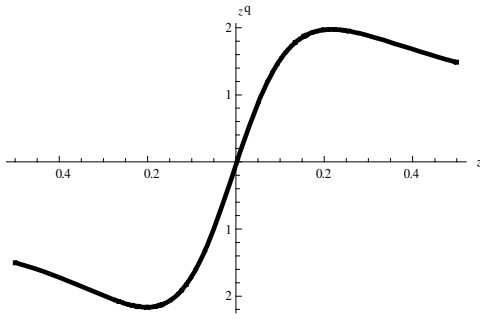


Figure 9-1: Attack defense $q^z(0,0,z)$

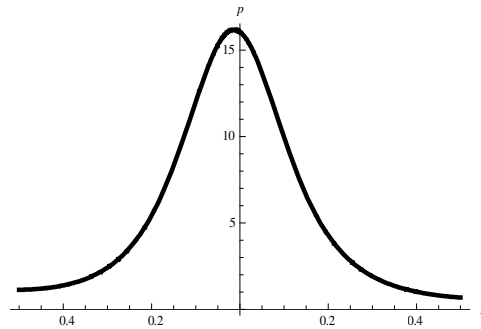


Figure 9-2: Attack defense $p(0,0,z)$

The key to achieving this is to focus not on the game value but on the *player strategy bias field*, f^j_{ov} . Up to now we have assumed that the two are simply related as in Eq. (8.62), allowing for slight discrepancies due to the orthogonalization process. We have assumed that the null space of the payoff vector is always related to the Nash equilibrium. This assumption however does not lead to *locked behavior*. We see no reason to hold on to that assumption. We can choose the *player strategy bias field* independently from the equilibrium flow, which leaves us free to set the form of the flow at what we have designated as the *still point*. We are also free to choose the player strategy bias field to conform to our expectations for the growth of the *player interest* along the various strategic directions.

As an example, we modify “Red” so that the payoff sees a different value for attacking the two sites:

$$G_{\text{Red}} = \frac{1}{10} \begin{pmatrix} 0 & 1 \\ 2 & 0 \end{pmatrix} \quad (9.3)$$

As a consequence we try a different *still point* equilibrium based on what each force sees:

$$V^a \propto \left\{ \frac{2}{3} \quad \frac{1}{3} \quad \frac{1}{4} \quad \frac{3}{4} \quad 4 \right\} \quad (9.4)$$

The order of indices has “Red” first and “Blue” second. The proportionality constant is adjusted so that the flow is a unit vector; as before we rescale the payoff by $\frac{1}{10}$.

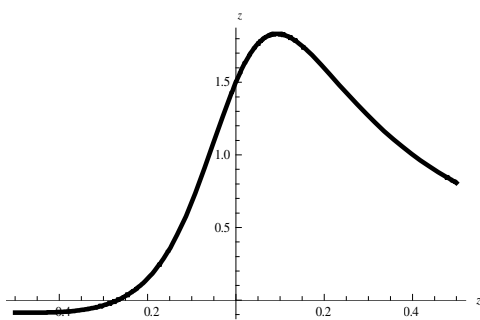


Figure 9-3: Attack defense $\Theta^z(0,0,z)$

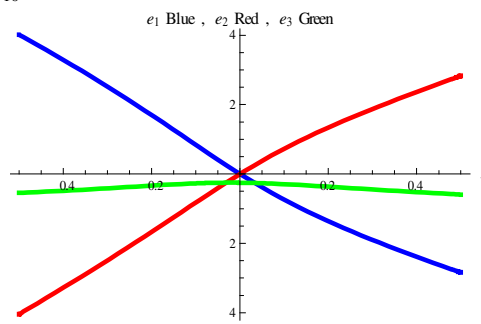


Figure 9-4: Attack defense e^α

If we choose the *player strategy bias field* independently, we add an amount, the *player interest* for each player that represents that *player's interest*, which for our numerical example in this section is 8 units for each player (Cf. section 8.12, exercise 20 as well as the exercises at the end of this chapter). This *locks* the pressure and acceleration as well as provides a distinct look for the compression (Figure 9-3) and engagement (Figure 9-4). In particular, “Blue” and “Red” exhibit strong player engagement away from the *still point*, even though they are “entitled” at the *still point*.

9.3 Decision flow

In this section we provide suitable initial starting points for *free fall* solutions (section 8.12, exercise 20). Conceptually, we start with the *quasi-stationary* solutions Eq. (9.7) from exercises 1-2 associated

with linear growth of the coordinates in Eq. (8.1) and no *harmonic* terms $U_{\sigma}^a = V_{\sigma}^a = 0$. Such solutions can be evolved to *free fall* solutions (exercises 1-19), leading to the *known-condition-based* behaviors, Figure 9-5 and Figure 9-6. The corresponding streamlines are straight lines as seen in the normal coordinate frame $\{u_1 \ u_2 \ u \ t\}$ of active variables.

Though the behavior is *free fall* on the hypersurface $z=0$, away from the hypersurface there are *acceleration* effects for the active metric components. See for example exercise 11. We can make other choices that lead to a *harmonic* spectrum or summation over multiple *harmonics* of the form Eq. (8.1). We thus obtain exact solutions of *free fall* and *acceleration* that were proposed previously (Thomas G. H., 2006), corresponding to situations in which the metric components are not constant and the initial conditions arbitrary. See exercises 10 and 13.

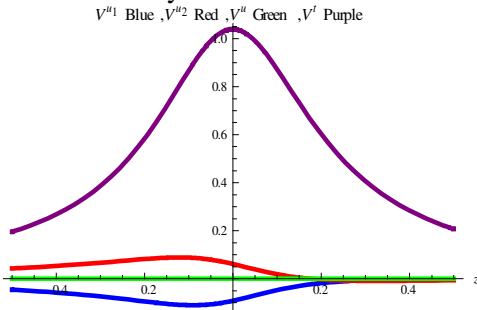


Figure 9-5: Attack defense flows
 $V^a(0,0,z)$

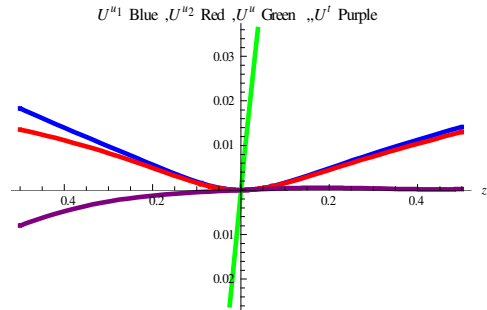


Figure 9-6: Attack defense intercepts
 $U^a(0,0,z)$

The *free fall* behavior in which some rotation is possible and replaces or becomes our assumption of *Nash equilibrium* (Figure 9-7), arises from the initial flows and the construction of an orthonormal set of vectors using the Gram-Schmidt process, section 8.2:

$$E^{j,a,t}_{\alpha,v,o} = \left(\begin{array}{c|ccc|ccc|c} \mu/\alpha & \alpha_1 & \alpha_2 & \alpha_3 & x & y & z & o \\ \hline \xi_1 & 1 & 0 & 0 & 0 & 0 & 0 & 0 \\ \xi_2 & 0 & 1 & 0 & 0 & 0 & 0 & 0 \\ r & 0 & 0 & 1.03318... & 0 & 0 & 0 & 0.25976... \\ \hline u_1 & 0 & 0 & -0.02309... & 1.00394... & 0 & 0 & -0.09184... \\ u_2 & 0 & 0 & 0.01539... & -0.00524... & 1.00174... & 0 & 0.06122... \\ u & 0 & 0 & 0 & 0 & 0 & 1 & 0 \\ \hline t & 0 & 0 & 0.26124... & -0.08904... & 0.05902... & 0 & 1.03906... \end{array} \right) \quad (9.5)$$

These initial conditions set the vectors of the *harmonic* flow, Eq. (8.81), Figure 9-9, Figure 9-10, Figure 9-11, and Figure 9-12. Although we obtain streamlines for the flow that are constant, for the other frame transformations E^a_v we get *harmonic* behaviors. We also get *harmonic* behaviors when $z \neq 0$, such as Figure 9-8 and Figure 9-27 (exercise 13).

The Dynamics of Decision Processes

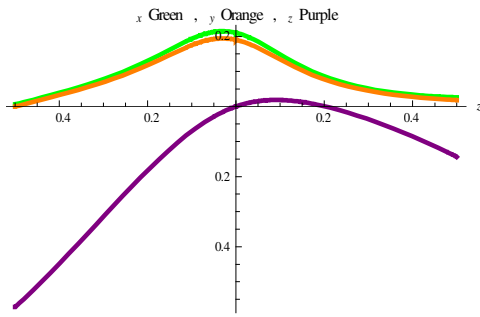


Figure 9-7: Attack defense composite payoff $\omega(0,0,z)$

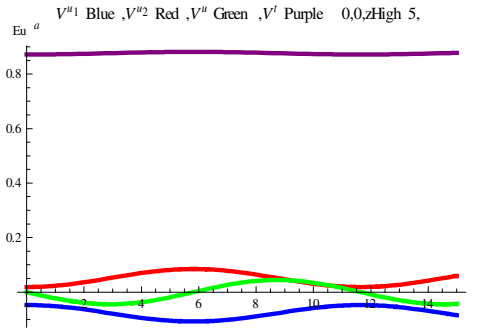


Figure 9-8: Harmonic attack-defense flow vectors $V^a(0,0,1/10,\tau)$

The initial attack-defense *harmonic* behaviors for the frame transformations reflect the boundary conditions we impose as part of the known conditions. We see that at time $\tau=0$, we align x with u_1 (Figure 9-9), y with u_2 (Figure 9-10), z with u (Figure 9-11) and o with t (Figure 9-12). In each case the corresponding “diagonal” transformation starts at 1.0. The orthogonalization process, Eq. (9.5) and the transformation equations between gradients and the frame transformation, Eq. (4.130) determine the remaining components.

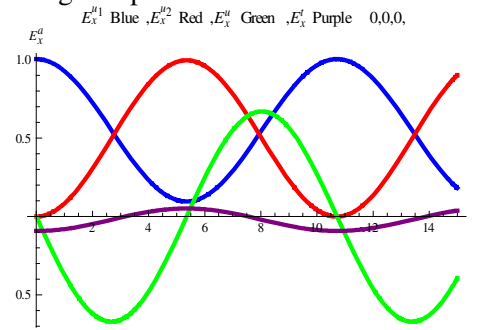


Figure 9-9: Frame transformations $E_x^a(0,0,0,\tau)$ for attack-defense model

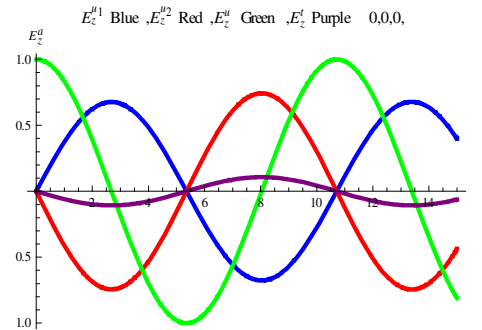


Figure 9-11: Frame transformations $E_z^a(0,0,0,\tau)$ for attack-defense model

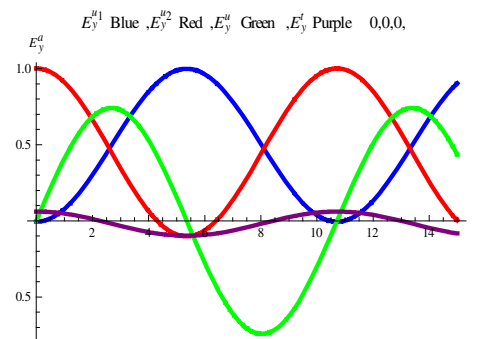


Figure 9-10: Frame transformations $E_y^a(0,0,0,\tau)$ for attack-defense model

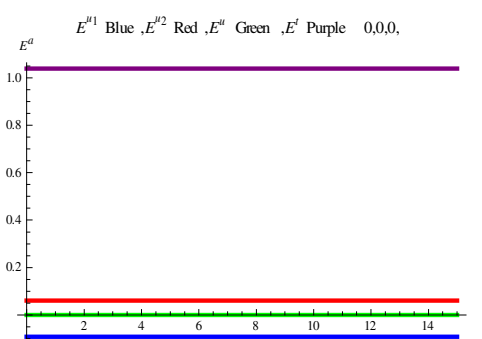


Figure 9-12: Frame transformations $E_o^a(0,0,0,\tau)$ for attack-defense model

In the rest of this section we expand upon the known conditions that determine our attack-defense *free fall* solutions. In the exercises, we suggest how to include additional acceleration effects that can be added on top of the *free fall* solutions.

9.4 Outcomes

In this chapter the student will have learned from the exercises how to compute the time dependence of the quasi-stationary player fixed frame solutions of the attack-defense model. It is an archetype of how to apply decision process theory to decision processes. Some of the key ideas from this chapter, especially the exercises, are:

- Locked behaviors
- Linear flows
- Free fall harmonics
- System harmonics
- Composite payoffs
- Streamline surfaces as seen in the normal coordinate basis
- Time behavior of pressure contours
- How to set the gauge and solve the associated partial differential equations
- The allowed physical region for streamlines.

9.5 Exercises

1. Starting with the linear *harmonic* Eq. (4.96) that leads to Eq. (4.97), show that with the gauge condition Eq. (4.136) and the divergence Eq. (8.10) of the acceleration, we have the following equations in the *co-moving orthonormal basis*:

$$\partial_\nu \partial^\nu U_0^a - (q^\nu + \Theta^\nu) \partial_\nu U_0^a + 4a^\nu \partial_\nu V_0^a - 2(\Theta^\nu + 3q^\nu) a_\nu V_0^a = 0$$

$$\partial_\nu \partial^\nu V_0^a - (3q^\nu + \Theta^\nu) \partial_\nu V_0^a + \left(2\omega_{\nu\alpha} \omega^{\nu\alpha} + \omega_{\nu\nu'} \omega^{\nu\nu'} + q_\nu q^\nu - \kappa \left(\mu + p - \frac{\mu - p}{n-1} \right) \right) V_0^a = 0 \quad (9.6)$$

2. In the notation of the 3+1 model, show that the equations for exercise 1 in the *co-moving orthonormal basis* are:

$$\nabla^2 U_0^a - (\Theta + \mathbf{q}) \cdot \nabla U_0^a + 4\mathbf{a} \cdot \nabla V_0^a - 2(\Theta + 3\mathbf{q}) \cdot \mathbf{a} V_0^a = 0$$

$$\nabla^2 V_0^a - (\Theta + 3\mathbf{q}) \cdot \nabla V_0^a + \left(\kappa \left(\mu + p - \frac{\mu - p}{n-1} \right) + \mathbf{q} \cdot \mathbf{q} + \frac{1}{2} \mathbf{I}_a \cdot \mathbf{I}^a - 2\boldsymbol{\omega} \cdot \boldsymbol{\omega} \right) V_0^a = 0 \quad (9.7)$$

3. Redo the attack defense model of section 9.1 with an initial vorticity vector $\omega_\nu = \{0, 0, \frac{4}{5}\}$. Show that the resultant vorticity Figure 9-13 is what you would expect. Show that the resultant pressure Figure 9-14 shows evidence that the *locked* behavior is substantially modified. How does a non-zero vorticity at the still point change the value of the *characteristic potential*? How do you modify Eq. (8.82) to allow for non-zero initial vorticity? What does it mean to have a non-zero vorticity, if we argue that at the *still point*, the players are not engaged and are entitled? Can we have *still points* where the pressure is a minimum as opposed to a maximum?

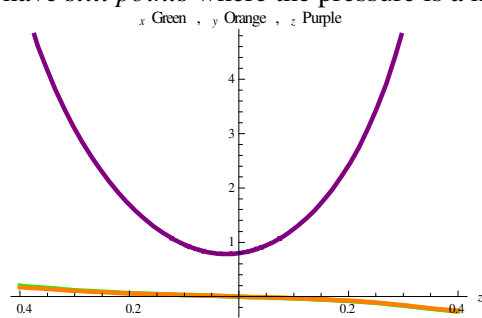


Figure 9-13: Composite payoff $\omega_\nu(0, 0, z)$ with initial spin

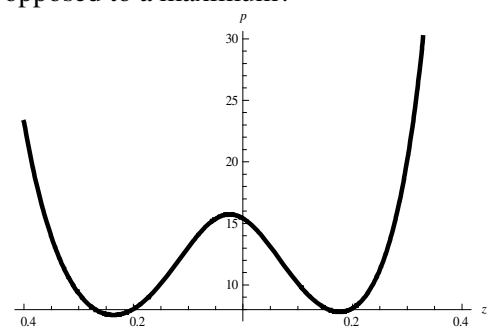


Figure 9-14: Pressure $p(0, 0, z)$ with initial spin

The Dynamics of Decision Processes

4. Starting with the *quasi-stationary harmonic* Eq. (4.100) that leads to Eq. (4.140), show that with the gauge condition Eq. (4.136) and the divergence Eq. (8.10) of the acceleration, we have the following equations in the *co-moving orthonormal basis* that determine the position scalars in terms of *harmonics*:

$$\begin{aligned}
 x^a(v, \tau) &= \sum_n X_n^a(v) \tau^n \\
 x^a(v_0, \tau) &= U_0^a(v_0) + V_0^a(v_0) \tau + \sum_{\sigma} (U_{\sigma}^a(v_0) \cos_N \varpi \tau + V_{\sigma}^a(v_0) \sin_N \varpi \tau) \\
 \partial_v x^a(v_0, \tau) &= \partial_v U_0^a(v_0) + \partial_v V_0^a(v_0) \tau + \sum_{\sigma} (\partial_v U_{\sigma}^a(v_0) \cos_N \varpi \tau + \partial_v V_{\sigma}^a(v_0) \sin_N \varpi \tau) \\
 X_{2m}^a(v_0) &= \delta_{m0} U_0^a(v_0) + (-)^m \sum_{\sigma} U_{\sigma}^a(v_0) \frac{\varpi^{2m}}{(2m)!} \\
 X_{2m+1}^a(v_0) &= \delta_{m0} V_0^a(v_0) + (-)^m \sum_{\sigma} V_{\sigma}^a(v_0) \frac{\varpi^{2m+1}}{(2m+1)!} \tag{9.8} \\
 X_{N+1} &= X_{N+2} = 0 \\
 n &= N, N-1, N-2, \dots, 0
 \end{aligned}$$

$$\left(\begin{aligned}
 &-\partial_v \partial^v X_n^a + (\Theta^v + (2n+1)q^v) \partial_v X_n^a + (n+2)(n+1)(1 + e_{\alpha} e^{\alpha} + 4a^v a_v) X_{n+2}^a \\
 &+ n \left(\kappa \left(\mu + p - \frac{\mu - p}{n-1} \right) - nq^v q_v - \omega_{vv'} \omega^{vv'} - 2\omega_{v\alpha} \omega^{v\alpha} \right) X_n^a \\
 &- 4(n+1)a^v \partial_v X_{n+1}^a + 2(n+1)(\Theta^v + (2n+3)q^v) a_v X_{n+1}^a
 \end{aligned} \right) = 0$$

5. For 3+1 dimensions, write the recursion in Eq. (9.8) in vector form:

$$\left(\begin{aligned}
 &\nabla^2 X_n^a - (\Theta + (2n+1)\mathbf{q}) \cdot \nabla X_n^a + (n+2)(n+1)(1 + e_{\alpha} e^{\alpha} - 4\mathbf{a} \cdot \mathbf{a}) X_{n+2}^a \\
 &+ n \left(\kappa \left(\mu + p - \frac{\mu - p}{n-1} \right) + n\mathbf{q} \cdot \mathbf{q} - 2\omega \cdot \omega + \frac{1}{2} \mathbf{I}_a \cdot \mathbf{I}^a \right) X_n^a \\
 &+ 4(n+1)\mathbf{a} \cdot \nabla X_{n+1}^a - 2(n+1)(\Theta + (2n+3)\mathbf{q}) \cdot \mathbf{a} X_{n+1}^a
 \end{aligned} \right) = 0 \tag{9.9}$$

6. For solutions to problem 5, show that the initial conditions can be set at $z = 0$ by specifying the coordinate and frame transformations:

$$\begin{aligned}
 x^a &= \sum_{n=0}^N X_n^a \tau^n \\
 E^a_o &= \sum_{n=0}^N n X_n^a \tau^{n-1} \\
 E^a_v &= \sum_{n=0}^N \partial_v X_n^a \tau^n + (2a_v - \tau q_v) E^a_o \tag{9.10} \\
 x^a(x, y, 0, 0) &= X_0^a(x, y, 0) \\
 E^a_o(x, y, 0, 0) &= X_1^a(x, y, 0) \\
 E^a_z(x, y, 0, 0) &= \partial_z X_0^a(x, y, 0) + 2a_z(x, y, 0) X_1^a(x, y, 0)
 \end{aligned}$$

7. As an application of the attack-defense model of section 9.1, the following streamline surfaces (Figure 9-15 and Figure 9-16) were obtained using the *quasi-stationary solutions* generated by Eq. (9.9) with appropriate boundary conditions and the common *free fall* components, sections 8.7 and 9.3. At the origin, the horizontal lines are the streamlines; the vertical lines move along

the transverse direction z . Can you explain the origin of the various behaviors? We provide the model parameters below in the *co-moving orthonormal basis* (Cf. section 9.1):

$$x^a = \text{freeFall}^a + U_0^a + V_0^a \tau + V_{10}^a \sin_N 10\tau + U_{10}^a \cos_N 10\tau = \sum X_n^a(x, y, 0) \tau^n$$

$$\partial_z x^a = \text{freeFall}_z^a + \sum Y_n^a(x, y, 0) \tau^n$$

$$V_{10}^a(x, y, 0) = \{-0.02 \quad 0 \quad 0 \quad -0.005\}$$

$$U_{10}^a(x, y, 0) = \{0 \quad -0.02 \quad -0.02 \quad 0\}$$

$$X_0^a(x, y, 0) = \left\{ \begin{array}{ccc} \left(\begin{array}{c} 1.59783 \sin \frac{\pi x}{5} \\ -0.008351 \sin \frac{\pi y}{5} \end{array} \right) & 1.59432 \sin \frac{\pi y}{5} & 0 \left(\begin{array}{c} -0.14617 \sin \frac{\pi x}{5} \\ +0.0974469 \sin \frac{\pi y}{5} \end{array} \right) \end{array} \right\} \quad (9.11)$$

$$X_1^a(x, y, 0) = \left\{ \begin{array}{ccc} -0.0918415 & 0.0612277 & \left(\begin{array}{c} -0.625869 \sin \frac{\pi x}{5} \\ +0.692672 \sin \frac{\pi y}{5} \end{array} \right) \\ & & 1.03907 \end{array} \right\}$$

$$Y_0^a(x, y, 0) = \{-0.000406996 \quad 0.000271331 \quad 1 \quad 0.00460464\}$$

$$Y_1^a(x, y, 0) = \{0.393702 \quad -0.433737 \quad 0 \quad -0.0233539\}$$

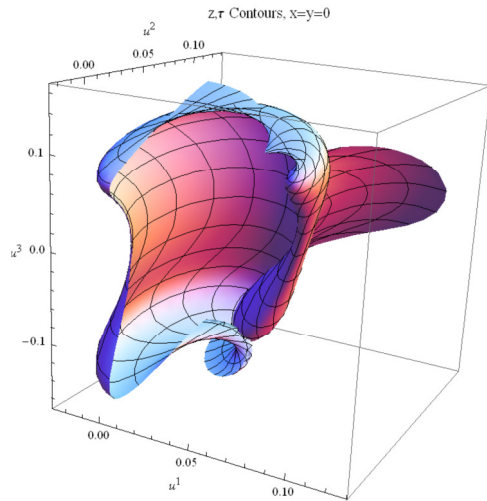


Figure 9-15: Streamline surfaces for $x = y = 0$.

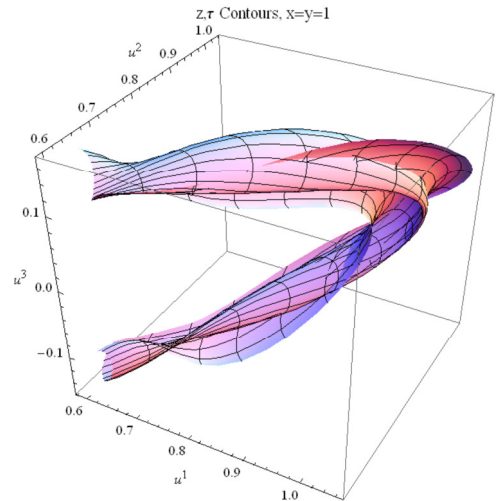


Figure 9-16: Streamline surfaces for $x = y = 1$.

The Dynamics of Decision Processes

8. Verify that the oscillatory structure displayed (Figure 9-15 and Figure 9-16) has its origin in our imposed *acceleration behavior* of the initial conditions, seen in Figure 9-17 and Figure 9-18:

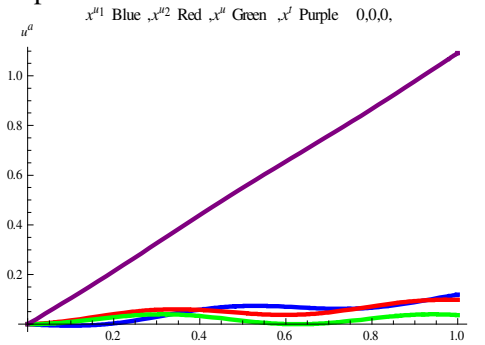


Figure 9-17: Coordinate vectors as a function of proper time τ . The legend is that Blue, Red, Green and Purple correspond to $\{x^{u_1}, x^{u_2}, x^u, x^t\}$ respectively.

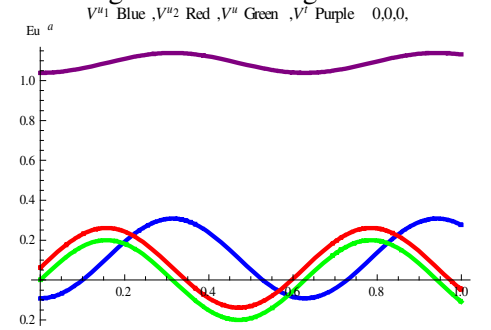


Figure 9-18: Flow vector in the normal frame coordinate system as a function of proper time τ . The legend is that Blue, Red, Green and Purple correspond to $\{E^{u_1}_o, E^{u_2}_o, E^u_o, E^t_o\}$ respectively.

9. For the Attack-Defense model of section 9.1 and exercises 7 and 0, explain why the streamline surface changes shape when we go to $x = -y = 1$, Figure 9-19. Compare the contour shapes of Figure 9-20 with the prisoner dilemma quantity in 1+1 dimension, Figure 5-48 and explain the origin of the similarities and differences. In both figures, which lines are constant z and which are constant τ ?

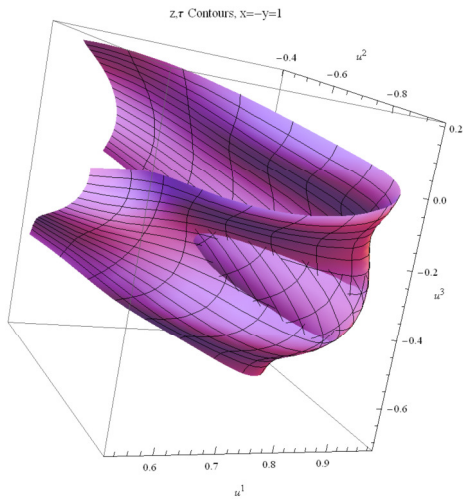


Figure 9-19: Streamline surfaces $x^a(1, -1, z, \tau)$.

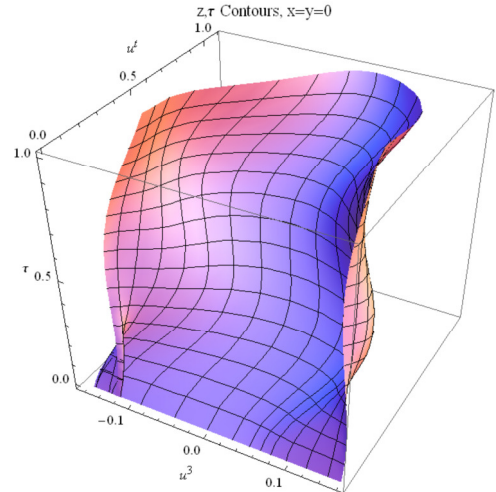


Figure 9-20: Proper time τ plotted parametrically against $x^u(0, 0, z, \tau)$ and $x^t(0, 0, z, \tau)$ showing constant (z, τ) streamlines.

10. In the previous Attack-Defense problems (exercise 7, 0 and 9), we have assumed that the primary oscillations were *acceleration effects*, not *free fall* behavior. Explain why the structures Figure 9-21 and Figure 9-22 follow from the model based on streamline flow (Thomas G. H., 2006, p.

124). Note that the structures assume that the payoff and most but not all metric components are constant along the streamline as seen in Eq. (1.75), which can be re-expressed using Eq. (3.32) showing the possibility of helical behavior because of feedback loops both between the time components and space components as well as between the space components:

$$\begin{aligned} \Delta_o E^a_o &= (q_v + \frac{1}{2} \Delta_v \gamma_{jk} E^j_o E^k_o + E_{ko} f^k_{vo}) E^{av} - \bar{\omega}^a_{bc} E^b_o E^c_o \\ \Delta_o E^a_v &= (\frac{1}{2} (1 + e_\alpha e^\alpha) E_{ko} f^k_{ov} - q_v - \omega_v^\alpha e_\alpha) E^a_o - (\omega_{vv'} + \frac{1}{2} E_{ko} f^k_{vv'}) E^{av'} - \bar{\omega}^a_{bc} E^b_v E^c_o \quad (9.12) \\ \Delta_v E^a_{v'} &= (\omega_{vv'} - e_\alpha \omega^\alpha_{vv'}) E^a_o - \bar{\omega}^a_{bc} E^b_v E^c_{v'} \end{aligned}$$

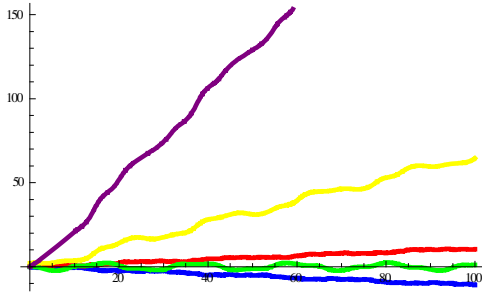


Figure 9-21: Streamline flow (Thomas G. H., 2006, p. 124) for $x^1 - x^2$, $x^3 - x^4$, $x^1 + x^2 - x^3 - x^4$, $x^1 + x^2 + x^3 + x^4$ and x' , which are blue, red, green, yellow and purple, respectively.

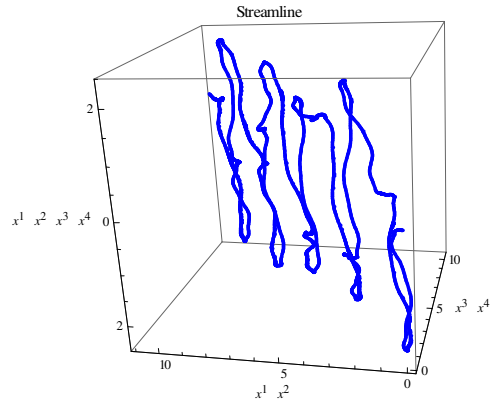


Figure 9-22: Streamline plot corresponding to flows (Thomas G. H., 2006, p. 124)

- Given that a common attribute of streamline equations from decision process theory solutions in (Thomas G. H., 2006) are helical in nature, we are motivated to assume that *quasi-stationary solutions* should also display helical structure without imposing the acceleration inputs. Using the previous Attack-Defense problems (exercise 7-9) as a starting point, we take out the acceleration effects (we reduce the weight 0.02 to zero) leaving only the *free fall* behavior (exercises 17-20 in section 8.12 and exercise 12 below), we obtain Figure 9-23. Note the helical solutions in Figure 9-24. Given the *free fall* nature, why are there any oscillations?

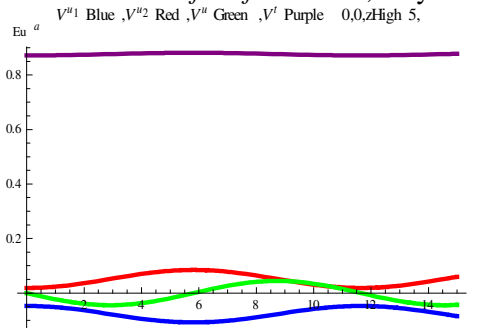


Figure 9-23: Free fall harmonic flows at $z = \frac{1}{10}$ for the attack-defense model

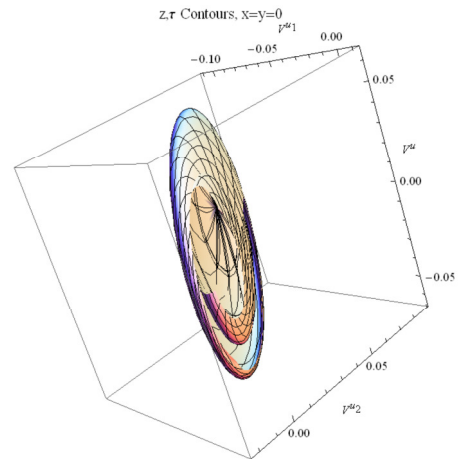


Figure 9-24: Attack-defense streamline flow contours for free fall behavior.

The Dynamics of Decision Processes

12. We use the eigenfrequency and eigenvalues of Eq. (8.80) for the attack defense model, along with an initial *composite payoff* vector along the x axis. Away from the still point, we expect acceleration forces to add non-trivial and additional path dependence along the streamlines, which can be resolved into harmonics. The simplest case is in which there are no acceleration forces $Q_v = 0$ along an initial streamline and no additional harmonics. This generates harmonic solutions such as Figure 9-25. We obtain streamline contours such as Figure 9-26, which are computed using the full equations. Identify the streamlines in the figure and explain the differences between this solution and the solution shown in exercise 7. Note the change in time scales. Are all streamlines in free fall with no acceleration?

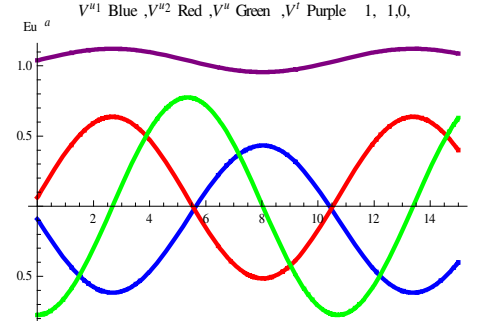


Figure 9-25: Initial flow with $Q_v = 0$ for the attack defense model. The legend is Blue, Red, Green and Purple, for $\{E^{u_1}_o, E^{u_2}_o, E^{u_3}_o, E^t_o\}$.

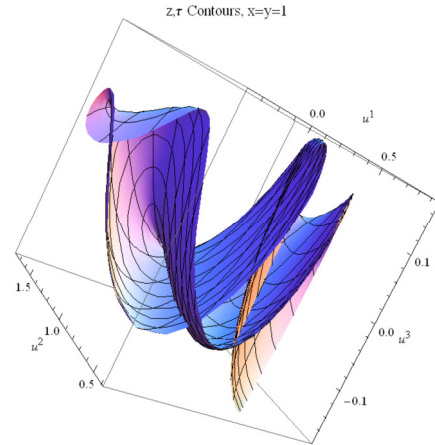


Figure 9-26: Streamline contours for *free fall* $Q_v = 0$ for the attack defense model. Strategic space components are $u^1 = u^{u_1}$, $u^2 = u^{u_2}$ and $u^3 = u^u$.

13. Based on section 8.12, exercise 20, we obtain other interesting contours, Figure 9-27 and Figure 9-28. Discuss and explain the differences and similarities of these with the corresponding case where the acceleration behaviors dominate.

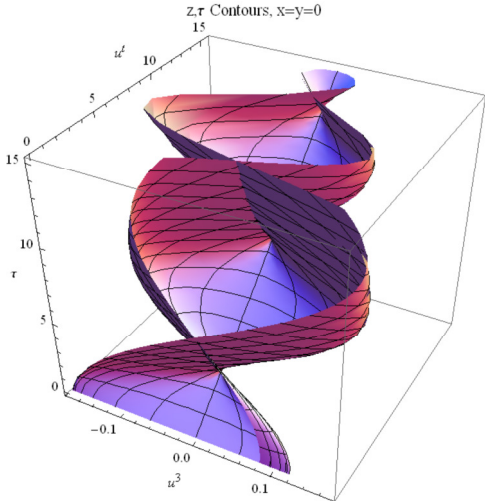


Figure 9-27: *Free fall* behavior of proper time τ

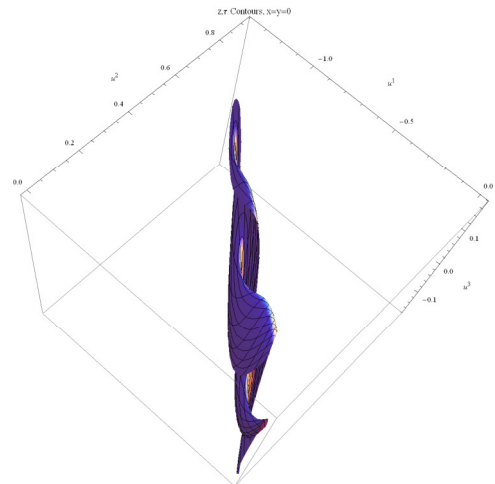


Figure 9-28: Streamline contours for *free fall*

14. Again using section 8.12, exercise 20, we obtain can investigate the behavior of the player charges as functions of time and $u = u^3$, which we call **player aggression**. When it is positive, player 1 is more involved than player 2. When it is negative, the situation is reversed. For the “blue” defense player in the attack-defense scenario, we see that there are limits to the size of the aggression, Figure 9-29. We see a similar limitation for “red” attack in Figure 9-30. What are the sources of these limitations? The contours are for fixed values of $\{x \ y\}$. Does the situation change if we vary these values? The behavior for the code of conduct is quite different, Figure 9-31. Explain the source(s) of the differences.

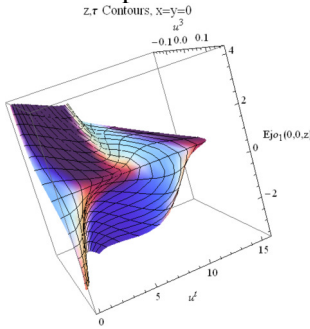


Figure 9-29: Blue (defense) charge

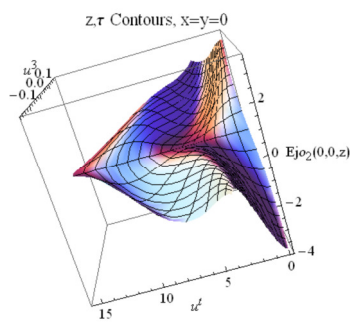


Figure 9-30: Red (attack) charge

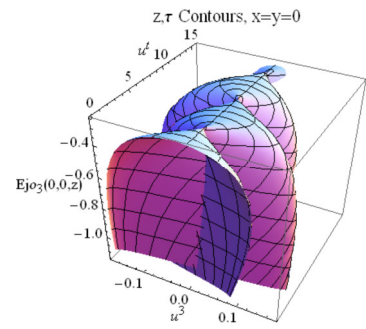


Figure 9-31: Code of Conduct charge

15. We gain additional insight into the behavior of decision processes by studying the contours of constant pressure, analogous to the insight gained in weather forecasting, as well as studying contours of constant acceleration. Using section 8.12, exercise 20, we provide examples of these behaviors, Figure 9-32 and Figure 9-33, respectively. At each instant of time, describe the forces that these contours represent.

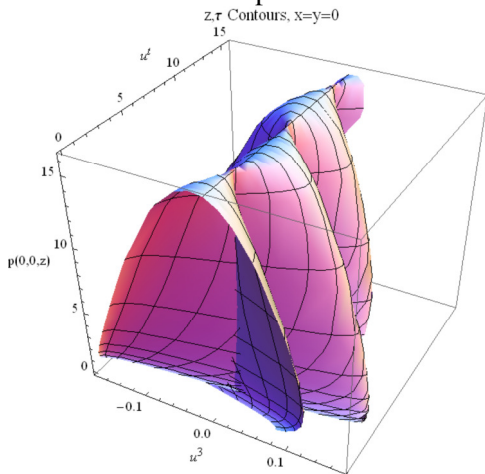


Figure 9-32: Constant pressure contours

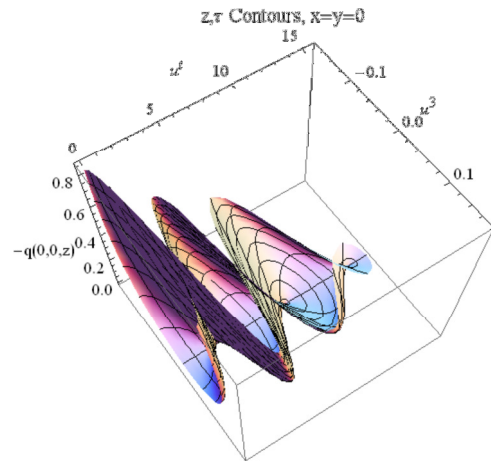


Figure 9-33: Constant acceleration contours

16. In the numerical work (e.g. Exercise 17), the assumption has been that we can set the **active acceleration** to zero at a point. Take this idea one step further. In a consistent way, set the active acceleration to zero on the initial surface (Cf. Exercise 14). Show that this implies that the acceleration and its gradient along the focused direction are determined on the surface:

$$\begin{aligned}
 q|_{pulse} &= -\frac{1}{2} \ln(1 + e^\gamma e_\gamma) \\
 q_z|_{pulse} &= \left(-e^\alpha I_{z\alpha} - e^\alpha \omega_{z\alpha\beta} e^\beta \right)_{pulse}
 \end{aligned}
 \tag{9.13}$$

The Dynamics of Decision Processes

17. In setting the active acceleration to zero on an initial surface, for numerical purposes you might think that Eq. (9.13) complicates the analysis using the *harmonic power series approximation* (Cf. Exercise 17). By investigating the numerical results in a variety of models for different mesh sizes, show that this is not the case. For example, we have computed the following table of results with an assumed set of initial conditions for the known conditions, using gauge invariance to set the initial value $a_z(0,0)$ (on the initial surface $z = 0$) of the *characteristic potential* to zero. These parameters characterize the limit cycle surface in the three dimensional space of $\{\partial_x a_z(x, y) \quad \partial_y a_z(x, y) \quad a_z(x, y)\}$. The *mesh* is the order of the highest harmonic term.

Mesh	$\partial_x a_z(0,0)$	$\partial_y a_z(0,0)$	$a_z(0,0)$
2	-0.00269302	0.01295000	2.28104×10^{-5}
3	-0.00329713	0.00792091	2.53266×10^{-5}
4	-0.000593376	0.00192842	8.78227×10^{-6}
5	-0.000600421	0.00193321	8.76807×10^{-6}
6	-0.000606108	0.00198585	5.79125×10^{-6}
7	-0.000597663	0.00198603	6.45998×10^{-6}
8	-0.000597316	0.00198954	5.31362×10^{-6}
10	-0.000589397	0.00198488	5.91349×10^{-6}

18. For your numerical solutions in Exercise 17, investigate the stability of the topology of your solutions for different *mesh* sizes. Compare your results with our results shown below.

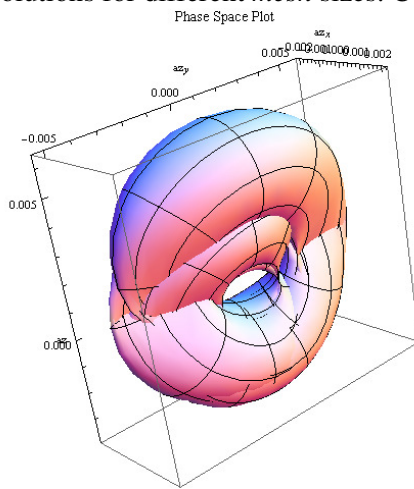


Figure 9-34: Gauge Condition Surface
mesh = 4 for: $\partial_x a_z \quad \partial_y a_z \quad a_z$

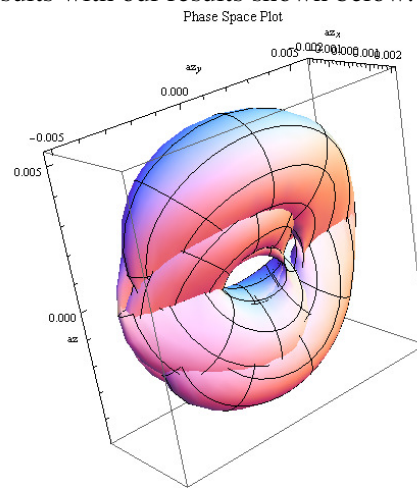


Figure 9-35: Gauge Condition Surface
mesh = 6 for: $\partial_x a_z \quad \partial_y a_z \quad a_z$

19. The *free fall* harmonic solutions in section 8.12 exercise 20 and section 9.5, exercises 13-18 display two interesting attributes: a linear solution and a helical solution that circulates around it. This is an inherent property of the *free fall* solution. Specifically it is a property of reflective of the value Ω_{vv} , Eq. (8.78). A general solution however, will start at an initial time from a known state over all spatial points. It can be represented as an infinite sum over harmonics. The time dependence of the general solution at $x = y = z = 0$ defines a solution that is no longer linear. Away from this “still point” will be fluctuations around this behavior. We may observe the inherent structure either from an exploration of different conditions at an initial time or from an exploration of different harmonic behaviors along $z = 0$. In this exercise we choose the latter. Consider the following curves with three harmonics, one of which is the *free fall* harmonic. The

behavior along $z = 0$ is now itself a helix, Figure 9-36, with additional rotational terms around it. The transverse directions are written as polar coordinates, $\{x = r \cos \theta, y = r \sin \theta\}$. The contours are for τ (yellow) and θ (purple). See if you can generate a model with similar behaviors. Note that the model predicts the behavior for $z \neq 0$, which means that the behavior at the initial time is now predicted.

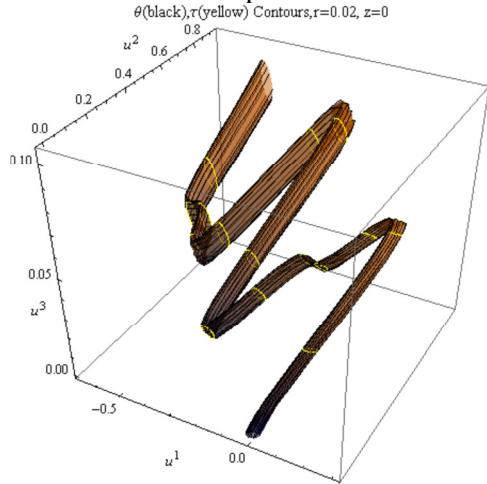


Figure 9-36: Three harmonic behavior in Normal Coordinates
 $\{u^1 \quad u^2 \quad u^3\}$

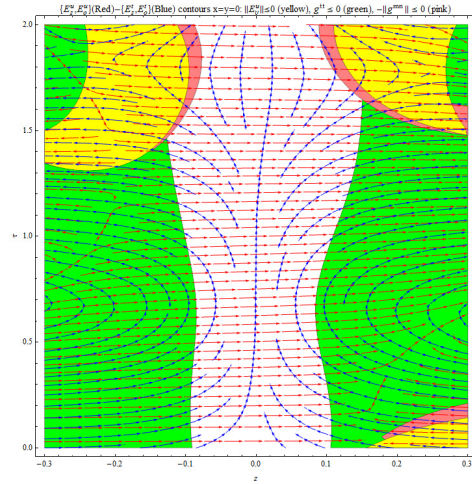


Figure 9-37: Frame Streamlines for three harmonic model

20. In Figure 9-37, the vectors represent the frame components $\{E_z^u, E_o^u\}$ (red) and $\{E_z^t, E_o^t\}$ (blue). The axes are $\{z, \tau\}$. Explain why three regions are **excluded**: the determinant $\|\tilde{E}_{v^n}^{u^m}\| \leq 0$ (yellow), $g'' \leq 0$ (green) and $g_{tt} = g\|g^{mn}\| \leq 0$ (pink). Compare your arguments to those in Section 5.13, Exercise 17. Also see the Exercises 1-4 in the following chapter, section 10.7.